Glucose-Stimulated Calcium Dynamics in Beta Cells From Male C57BL/6J, C57BL/6N, and NMRI Mice: A Comparison of Activation, Activity, and Deactivation Properties in Tissue Slices

Viljem Pohorec[1], Lidija Križančić Bombek[1], Maša Skelin Klemen[1], Jurij Dolenšek[1,2]* and Andraž Stožer[1]*

[1] Institute of Physiology, Faculty of Medicine, University of Maribor, Maribor, Slovenia, [2] Faculty of Natural Sciences and Mathematics, University of Maribor, Maribor, Slovenia

Although mice are a very instrumental model in islet beta cell research, possible phenotypic differences between strains and substrains are largely neglected in the scientific community. In this study, we show important phenotypic differences in beta cell responses to glucose between C57BL/6J, C57BL/6N, and NMRI mice, i.e., the three most commonly used strains. High-resolution multicellular confocal imaging of beta cells in acute pancreas tissue slices was used to measure and quantitatively compare the calcium dynamics in response to a wide range of glucose concentrations. Strain- and substrain-specific features were found in all three phases of beta cell responses to glucose: a shift in the dose-response curve characterizing the delay to activation and deactivation in response to stimulus onset and termination, respectively, and distinct concentration-encoding principles during the plateau phase in terms of frequency, duration, and active time changes with increasing glucose concentrations. Our results underline the significance of carefully choosing and reporting the strain to enable comparison and increase reproducibility, emphasize the importance of analyzing a number of different beta cell physiological parameters characterizing the response to glucose, and provide a valuable standard for future studies on beta cell calcium dynamics in health and disease in tissue slices.

Keywords: beta cell, mouse models, calcium imaging, glucose-dependence, tissue slice

INTRODUCTION

Laboratory mice are a vital source of islets of Langerhans in research on beta cell physiology, functional adaptation, and dysfunction during development of type 2 diabetes mellitus (T2DM) (1, 2), mostly due to their low housing costs, short breeding interval, availability for genetic manipulation, and regulatory requirements. From the translational point of view, despite some important differences

(3) the islets of Langerhans show many structural and functional similarities in mice and men (4, 5). Therefore, it is not surprising that mouse models of T2DM exhibit comparable disease characteristics and can provide a significant insight into the mechanisms of T2DM development in humans (2). However, the translational relevance (6) is not the only important aspect when it comes to mouse models of beta cells physiology and pathophysiology. Another very important aspect are possible differences between individual mouse models (7). More specifically, either genetically defined inbred strains (8) or genetically undefined outbred stocks (9) are available. Some advocate greater use of inbred strains, arguing that the reduced genetic variability and the concomitantly reduced phenotypic variation contribute to the power of experimental results (8–11). However, there is still uncertainty as to whether this is necessarily preferable, as comparable phenotypic variation has been demonstrated in inbred and outbred mice (12–14). Adding to the complexity is the fact that even substrains of the inbred strains can exhibit considerable phenotypic variation. The two most commonly used substrains – C57BL/6J and C57BL/6N, while descended from the parent strain C57BL/6, demonstrate genetic (15, 16) and phenotypic (16, 17) differences. One of the more pertinent differences in this regard is the nicotinamide nucleotide transhydrogenase (Nnt) gene, which encodes a mitochondrial enzyme involved in NADPH production (18) that harbors a mutation in the C57BL/6J substrain (19–21), whereas it remains intact in several C57BL/6N substrains (15). More specifically, at the phenotype level, examination of glucose handling in the two substrains yielded conflicting results. The NNT activity defect in C57BL/6J mice seems to be associated with attenuated glucose-stimulated insulin release (19, 22) compared to C57BL/6N mice (19, 22–24), while some report conflicting results for the two substrains (23–26). Moreover, the two substrains are differentially sensitive to diet-induced obesity (DIO). Both C57BL/6J and C57BL/6N are prone to DIO, which is manifested by a marked increase in body mass (24, 27, 28), impaired glucose tolerance (27–29), an increase in fasting blood glucose and serum insulin that develops later in C57BL/6J than C57BL/6N (28), decreased insulin release (29), and insulin resistance (24). For a more detailed comparison of DIO phenotypes in different C57BL/6 substrains, see (24). In contrast, the outbred NNT competent NMRI mice exhibit better glucose handling compared with the C57BL/6 strain. The NMRI mice were reported to clear glucose more efficiently than the C57BL/6J (30), resulting in normal glucose tolerance (31). Moreover, they seem to be less susceptible to DIO because (i) feeding with HFD or WD resulted in a smaller increase in body mass than in C57BL/6J (30) or C57BL/6N (13) mice and (ii) glucose tolerance was less impaired than in C57BL/6J mice (30). Since DIO induced a comparable degree of insulin resistance in NMRI and C57BL/6J mice, normoglycemia was probably maintained in NMRI mice due to concomitant hyperinsulinemia (30). In light of the above phenotypic differences among the mouse strains and substrains, one should be careful when generalizing findings on the molecular mechanisms obtained from a particular mouse substrain, and precise in reporting of said substrain (7, 32).

For insulin-secreting beta cells, intracellular calcium concentration ($[Ca^{2+}]_i$) remains a suitable surrogate for the study of molecular machinery responsible for insulin secretion, and the importance of $[Ca^{2+}]_i$ dynamics for pancreatic insulin secretion is well acknowledged (33–36). In general, stimulation of beta cells with glucose results in an initial transient increase in $[Ca^{2+}]_i$ in the first phase, followed by oscillatory changes in calcium influx in the second phase that persist until stimulation ceases (5, 35, 37). These changes in $[Ca^{2+}]_i$ are preceded by changes in membrane potential (38, 39) and drive insulin secretion (40, 41). Over the past century, numerous mouse models have been introduced to study $[Ca^{2+}]_i$ dynamics, most notably the genetically undefined outbred NMRI mice (37, 40, 42), and the Ob/Ob (Lep^ob) mice (41, 43, 44) derived from a non-inbred colony in the middle of the previous century. However, the last two decades have witnessed greater diversity in the use of mouse models, often using genetically defined inbred strains, such as the C57BL/6J (45, 46) and the C57BL/6N mice (47), as well as genetically modified mice with the C57BL/6J background (48–50). We recently quantified the concentration-dependence of the beta cell response to glucose using high-resolution multicellular $[Ca^{2+}]_i$ imaging in many beta cells in tissue slices (51), but only for the NMRI strain. Given an increasing use of inbred strains and related knock-out models in islet research, it is important to assess whether the genetic background in general and the Nnt mutation in specific influence glucose-stimulated $[Ca^{2+}]_i$ dynamics in beta cells.

In this study, we therefore aimed to characterize and compare beta cell $[Ca^{2+}]_i$ dynamics in the three today most commonly used mouse strains, i.e., the NNT-deficient inbred C57BL/6J mice, NNT-competent inbred C57BL/6N mice, and NNT-competent outbred NMRI mice. To increase the probability of detecting possible changes, a wide range of physiological (7–10 mM) and supraphysiological (12-16 mM) glucose concentrations were used to stimulate beta cells in islets of Langerhans in acute pancreas tissue slices and their responses to glucose were systematically analyzed over the whole response, i.e., during activation, plateau activity, and deactivation.

MATERIALS AND METHODS

Ethics Statement
The study was performed according to the European and National Legislation, Directive 63/2010/EU. The protocol was approved by the Administration for Food Safety, Veterinary Sector and Plant Protection of the Republic of Slovenia (approval number: U34401-12/2015/3 and U34401-35/2018-2). The study was conducted in strict accordance with all national and European recommendations pertaining to care and work with laboratory animals, and every effort was made to minimize animal suffering.

Animals
Experiments were performed on 12–13-week-old male C57BL/6J (RRID:IMSR_JAX:000664), C57BL/6N (RRID:IMSR_CRL:027),

and NMRI mice (RRID:IMSR_CRL:605), all acquired from Charles River. The mice were fed a standard rodent diet Ssniff Rat/mouse – Maintenance (V1534-000) (Ssniff, Soest, Germany) with 9, 24, and 67% of kcal derived from fat, protein, and carbohydrates, respectively, and water *ad libitum*. They were housed in individually ventilated cages (Allentown LLC, USA) in groups of 1-4 animals per cage at 20-24°C, 45-65% relative humidity, and a 12-hour day-night lighting cycle. Mice were weighed before sacrifice. Following the sacrifice with CO_2 and cervical dislocation, the mouse was placed on its abdomen, and body length was measured from the nose tip to the base of the tail. Glucose was measured within 5 minutes upon sacrifice in the morning between 8 AM and 9 AM from the tail vein using the Accu-Check Aviva glucometer (Roche, Switzerland). During analysis, body mass index (BMI) was calculated as the ratio between body weight and body surface area (g/m^2), where body surface area was calculated according to the following formula (52):

$$body\ surface\ area\ (m^2)$$

$$= 0.007184 \times (weight\ (kg))^{0.425} \times (height(cm))^{0.725} \quad (1)$$

Tissue Slice Preparation and Dye Loading

Acute pancreas tissue slices from C57BL/6J, C57BL/6N, and NMRI mice were prepared as described previously (53–55). In brief, after cervical dislocation of the animal, the abdominal cavity was accessed *via* laparotomy. The pancreas was injected with 1.9% low-melting-point agarose (Lonza Rockland Inc., USA) at the proximal common bile duct, which was clamped distally at the major duodenal papilla. The agarose was dissolved in extracellular solution (ECS) containing (in mM 125 NaCl, 26 NaHCO$_3$, 6 glucose, 6 lactic acid, 3 myo-inositol, 2.5 KCl, 2 Na-pyruvate, 2 CaCl$_2$, 1.25 NaH$_2$PO$_4$, 1 MgCl$_2$, 0.5 ascorbic acid) and maintained at 40°C. Immediately following the agarose injection, the pancreas was cooled with the ice-cold ECS, extracted from the animal, and placed in a Petri dish containing cooled ECS. The tissue was then cut into 3-5 mm^3 pieces, which were embedded in agarose and cut into 140 μm thick slices vibratome (VT 1000 S, Leica). The slices were transferred into a Petri dish containing HEPES-buffered saline (HBS, consisting of (in mM) 150 NaCl, 10 HEPES, 6 glucose, 5 KCl, 2 CaCl$_2$, 1 MgCl$_2$; titrated to pH=7.4 with 1 M NaOH) at room temperature. The prepared slices were stained in the dye-loading solution (6 μM Oregon Green 488 BAPTA-1 AM (OGB-1, Invitrogen), 0.03% Pluronic F-127 (w/v), and 0.12% dimethyl sulfoxide (v/v) dissolved in HBS) for 50 min at room temperature. All chemicals were obtained from Sigma-Aldrich (St. Louis, Missouri, USA) unless otherwise stated.

Experimental Protocol

Stained tissue slices were placed individually under the microscope into the recording chamber, which was continuously perifused with carbogenated ECS containing 6 mM glucose at 37°C. To stimulate the slices, we manually changed the perifusate to a single stimulatory glucose concentration (7, 8, 9, 10, 12 or 16 mM) dissolved in carbogenated ECS at 37°C for 40, 30, 20, 20, 15, and

15 min, respectively. After stimulation, the slice was reintroduced to the perifusate containing 6 mM glucose in ECS for at least 15 min.

Imaging of Intracellular Free Calcium Concentration Dynamics in Beta Cells

$[Ca^{2+}]_i$ imaging was performed using an upright confocal microscope system Leica TCS SP5 AOBS Tandem II with a 20X HCX APO L water immersion objective, NA 1.0, and an inverted confocal system Leica TCS SP5 DMI6000 CS with a 20X HC PL APO water/oil immersion objective, NA 0.7 (all from Leica Microsystems, Germany). The time series were acquired at a resolution of 512 X 512 pixels with a frequency of 2 Hz. The calcium reporter dye was excited with a 488 nm argon laser line, and the emitted fluorescence was detected with a Leica HyD hybrid detector in the 500-700 nm range (all from Leica Microsystems, Germany), as previously described (51, 54, 55).

Data Analyses

The cross-sectional areas of the islets were measured manually using high-resolution images (1024 X 1024 pixels) in the focal plane, where the $[Ca^{2+}]_i$ signals were recorded using LASX software (Leica Microsystems, Germany). For calcium dynamics analysis, regions of interest (ROI) were manually selected and exported using custom offline software (ImageFiltering, copyright Denis Špelič). Traces with considerable motion artifacts were excluded from further analysis, which was performed using in-house MATLAB scripts (The MathWorks, Inc., Massachusetts, USA, RRID: SCR_001622). A combination of linear and exponential fitting was used to account for the photobleaching effect. Activation times (i.e., the time delay from the onset of the stimulus to the transient increase in $[Ca^{2+}]_i$) and deactivation times (i.e., the time delay from the withdrawal of the stimulus to the last oscillation) for individual cells were determined manually using custom Matlab scripts. For the plateau phase of the beta cell responses, we binarized the oscillatory activity and defined the onset and termination of each oscillation at times of their half-maximal amplitudes using Matlab. The binarized signals were subsequently used to calculate the duration (i.e., the time interval between the onset and termination of a single oscillation), frequency (i.e., the inverse value of the interval between the onsets of two successive oscillations), and active time (i.e., the percentage of time occupied by oscillations). Active time (AT) is mathematically defined as the following product:

$$AT = f \cdot d \quad (2)$$

where f is the frequency (in Hz) and d is the duration (in seconds) of oscillations. Data were pooled across all cells and plotted using Tukey-style boxplots with whiskers denoting 1.5-times the interquartile range of the data. Statistical analyses were performed using GraphPad Prism 9.2 (GraphPad Software, Inc., San Diego, USA, RRID:SCR_002798). Statistical differences between groups were tested using one-way analysis of variance (ANOVA) on ranks, followed by Dunn's multiple comparison test, where data were not normally distributed, and one-way

analysis of variance (ANOVA), where data were normally distributed. Asterisks denote statistically significant differences, as follows: * p<0.05, ** p<0.01, *** p<0.001, and **** p<0.0001. Shifts in the dose-dependent activation curves were calculated assuming a sigmoid-shaped 4 parameter logistic mathematical model (56), according to the following equation:

$$y(x) = d + \frac{a - d}{1 + \left(\frac{x}{c}\right)^b} \qquad (3)$$

where delay in response $f(x)$ is expressed as a function of concentration x, parameters a and d denote the lower and upper asymptote, respectively, b the slope of the linear portion of the curve, and c (commonly termed EC50/IC50) concentration at response midway between a and d. To compare the curves, parameters were set such that the value of the correlation coefficient was $R^2 \geq 0.90$ for the individual fits through median delays ($b = -10.5$, $a = [100\ 200]$ s, and $d = 850$ s).
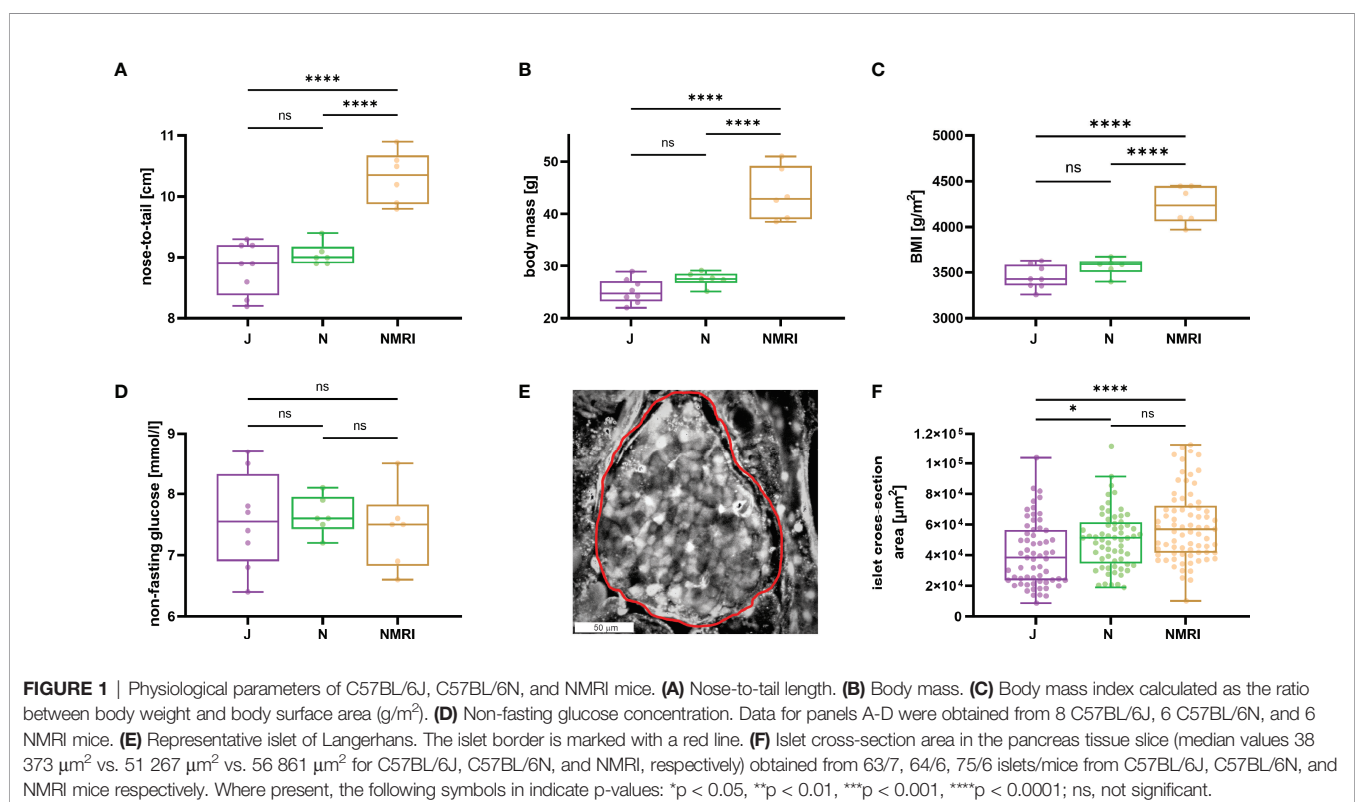
RESULTS

In the study of the (patho)physiology of the pancreas, the impact of differences between mouse (sub)strains is not yet fully understood. We therefore performed a systematic comparison between the three commonly used mouse strains, namely the C57BL/6J, C57BL/6N, and NMRI mice. We analyzed the beta cell (i) activation properties, (ii) oscillatory dynamics during the plateau phase of the response, and (iii) deactivation properties over a wide range of glucose concentrations. Additionally, we characterized the strains by using morphological measurements and by measuring non-fasting glucose.

Gross Morphological and Glucose-Handling Interstrain Differences

To describe the morphological differences between the strains, we measured body mass and nose-to-tail length. NMRI mice were larger (nose-to-tail length, median value 10.4 cm) and heavier (median value 42.9 g) than C57BL/6J (median length 8.9 cm and mass 24.8 g) and C57BL/6N mice (median length 9.0 cm and mass 27.5 g) mice (**Figures 1A, B**), whereas the two inbred strains showed no difference in nose-to-tail length and body mass. Additionally, the calculated body mass index (BMI) was statistically significantly larger in NMRI mice than in either of the B6 strain (**Figure 1C**). Non-fasted glucose levels did not differ between strains (median values 7.6, 7.6, and 7.5 mM for C57BL/6J, C57BL/6N, and NMRI, respectively) (**Figure 1D**). We also compared the gross morphology of the islets of Langerhans between C57BL/6J, C57BL/6N, and NMRI mouse strains (**Figures 1E, F**). Qualitatively, we found no differences in islet morphology between the three strains. To quantify the islet morphology, we measured the cross-sectional area of each islet in pancreas tissue slices that were subsequently designated for calcium imaging. Islets from the C57BL/6J mice were 33% smaller by median compared with the NMRI mice and had a median of 10% smaller cross-sectional area than the C57BL/6N mice, with no significant difference between the NMRI and C57BL/6N mice.

FIGURE 1 | Physiological parameters of C57BL/6J, C57BL/6N, and NMRI mice. **(A)** Nose-to-tail length. **(B)** Body mass. **(C)** Body mass index calculated as the ratio between body weight and body surface area (g/m²). **(D)** Non-fasting glucose concentration. Data for panels A-D were obtained from 8 C57BL/6J, 6 C57BL/6N, and 6 NMRI mice. **(E)** Representative islet of Langerhans. The islet border is marked with a red line. **(F)** Islet cross-section area in the pancreas tissue slice (median values 38 373 μm² vs. 51 267 μm² vs. 56 861 μm² for C57BL/6J, C57BL/6N, and NMRI, respectively) obtained from 63/7, 64/6, 75/6 islets/mice from C57BL/6J, C57BL/6N, and NMRI mice respectively. Where present, the following symbols in indicate p-values: *p < 0.05, **p < 0.01, ***p < 0.001, ****p < 0.0001; ns, not significant.

Calcium Response to Glucose Stimulation in the Three Mouse Strains

To assess the glucose-dependent properties of activation, plateau phase, and deactivation, we exposed the pancreas tissue slices of the three mouse strains to square-like pulses of stimulatory glucose in the physiological (7, 8, 9, 10 mM) and supraphysiological (12, 16 mM) ranges. A single stimulation was performed per tissue slice. The $[Ca^{2+}]_i$ dynamics were recorded in beta cells within the optical cross-section of the islet of Langerhans and showed a three-phase response consisting of an initial transient increase in $[Ca^{2+}]_i$ (activation), followed by a sustained increase with fast oscillations (plateau phase), and a decrease in $[Ca^{2+}]_i$ after cessation of stimulation (deactivation), as described previously (51).

The Activation Time Upon Stimulation With Glucose Is Delayed in C57BL/6J Mice

Beta cells exhibit a characteristic delay following glucose stimulation, a property that has been shown to depend on glucose concentration in the NMRI strain (51, 54). To identify differences between the three strains, we measured the delays between the onset of stimulation and initial $[Ca^{2+}]_i$ increase in individual beta cells (**Figure 2A**). Pooling data from several islets of the three strains demonstrated that the delays depended on the glucose concentration in all strains (**Figure 2B**). Regardless of strain, a general trend was observed, showing that an increase in glucose concentration decreased the median activation delay and that the threshold concentration of glucose was 7 mM. However, the absolute values differed between the three strains. Specifically, delays at most glucose concentrations were longest in the C57BL/6J mice and the shortest in the NMRI mice at all glucose concentrations. The difference in median delays to activation of C57BL/6J mice were by an average of 52.9% longer than in NMRI mice (85.6% 7 mM, 41.1% 8 mM, 50.8% 9 mM, 89.7% 10 mM, 28.4% 12 mM, and 21.4% 16 mM). The C57BL/6N strain generally showed an intermediate delay that was shorter than in C57BL/6J and longer than in NMRI mice (except at 7 mM and 8 mM glucose, where no difference was found relative to C57BL/6J in the former case and to NMRI mice in the latter). In relative terms, the difference in median delays to activation of C57BL/6N mice was on average 24.6% shorter than in the C57BL/6J strain. Still, no consistent ratio or trend was observed when comparing different concentrations (-6.4% 7 mM, 36.9% 8 mM, 41.0% 9 mM, 54.5% 10 mM, 0.4% 12 mM, and 20.9% 16 mM). In an attempt to quantify the above strain differences, we calculated the IC50 value (e.g., concentration, at which the delays shortened to 50% of maximal value) assuming a 4-parameter logistic model (56) (**Supplementary Figure 1**). The IC50 values were 8.1 mM (C57BL/6J), 7.8 mM (C57BL/6N), and 6.9 mM (NMRI), demonstrating that the dose-dependent curves of the two inbred strains were right-shifted by 0.9 - 1.2 mM relative to NMRI mice. In this context, we qualitatively observed that some islets of C57BL/6J mice failed to activate in 7 mM glucose in the given time period. However, we did not quantify this further, and the islets were excluded from the quantitative analysis.

We observed a relatively large heterogeneity of activation delays between individual cells of the same islet (**Figures 2A, B**).

Interquartile ranges were comparable between the inbred and outbred mouse strains. To quantitatively compare the variability among the three strains, we resorted to a robust measure of variability, the median absolute deviation (MAD). Absolute deviations of activation delays from the median were calculated per islet, and the median value of the pooled data was presented in **Figure 2C**. The heterogeneity of delays was dependent on glucose concentration, as previously reported for the NMRI strain (51). The MAD ranged from the largest values at the threshold concentration (380 s C57BL/6J, 296 s C57BL/6N, 184 s NMRI) to the smallest values at the highest concentration tested (31 s C57BL/6J, 25 s C57BL/6N, 28 s NMRI) (**Figure 2C**). Excluding the threshold glucose concentration, MAD did not differ substantially between inbred and outbred strains.

Increasing Glucose Concentrations Modulate the Plateau Activity Differently in the Three Strains of Mice

Following initial activation, beta cells exhibit repetitive oscillations of $[Ca^{2+}]_i$ that are superimposed on an elevated level of $[Ca^{2+}]_i$, a feature referred to as the plateau phase of the glucose response (37, 57). To look for possible differences between the three strains during the plateau phase, we measured the duration, frequency and amplitude of oscillations, as well as the active time, which indicates the proportion of time during which $[Ca^{2+}]_i$ is elevated (**Figure 3A**).

Remarkably, when comparing the three strains of mice, we found profound differences in the duration and frequency changes when expressed as a function of the glucose concentration used for stimulation (**Figures 3B, C**). Noteworthy, we failed to observe any systematic or biologically relevant differences in the amplitude of oscillations (**Supplementary Figure 2**). More specifically, beta cells from C57BL/6J mice responded to increasing glucose concentrations with an increase in oscillation frequency ranging from a median of 1.5 min⁻¹ at 7 mM to 9.9 min⁻¹ at 16 mM glucose. In stark contrast, the duration of oscillations remained range-bound to durations like those observed at the threshold concentration (median 2.5 - 3.0 s). The C57BL/6N strain, on the other hand, showed an inverse effect of increasing concentrations: a gradual increase in duration of oscillations rather than their frequency. More specifically, the duration increased from a median of 3.0 s at 7 mM to 9.6 s at 16 mM glucose, while the frequency varied between a median of 1.9 and 4.6 min⁻¹, with no clear trend. The NMRI strain, however, modulated active time with frequency in the physiological and with duration in the supraphysiological range of glucose concentration (the shift occurred at glucose concentrations of 9- and 10-mM). Frequency increased from a median of 2.3 min⁻¹ at 7 mM to 4.6 - 5.9 min⁻¹ at 9 - 10 mM glucose (durations were in the range of median 2.5 and 3.5 s with no clear trend). At glucose concentrations above 10 mM, the duration of oscillations increased to a median of 5.5 s, while the frequency of oscillations even decreased to 4.4 min⁻¹ at 16 mM glucose. When comparing islets from the same animal with islets from different animals and strains, a similar heterogeneity in frequency of oscillations was observed (**Supplementary Figure 3**). On the other hand, active time increased consistently
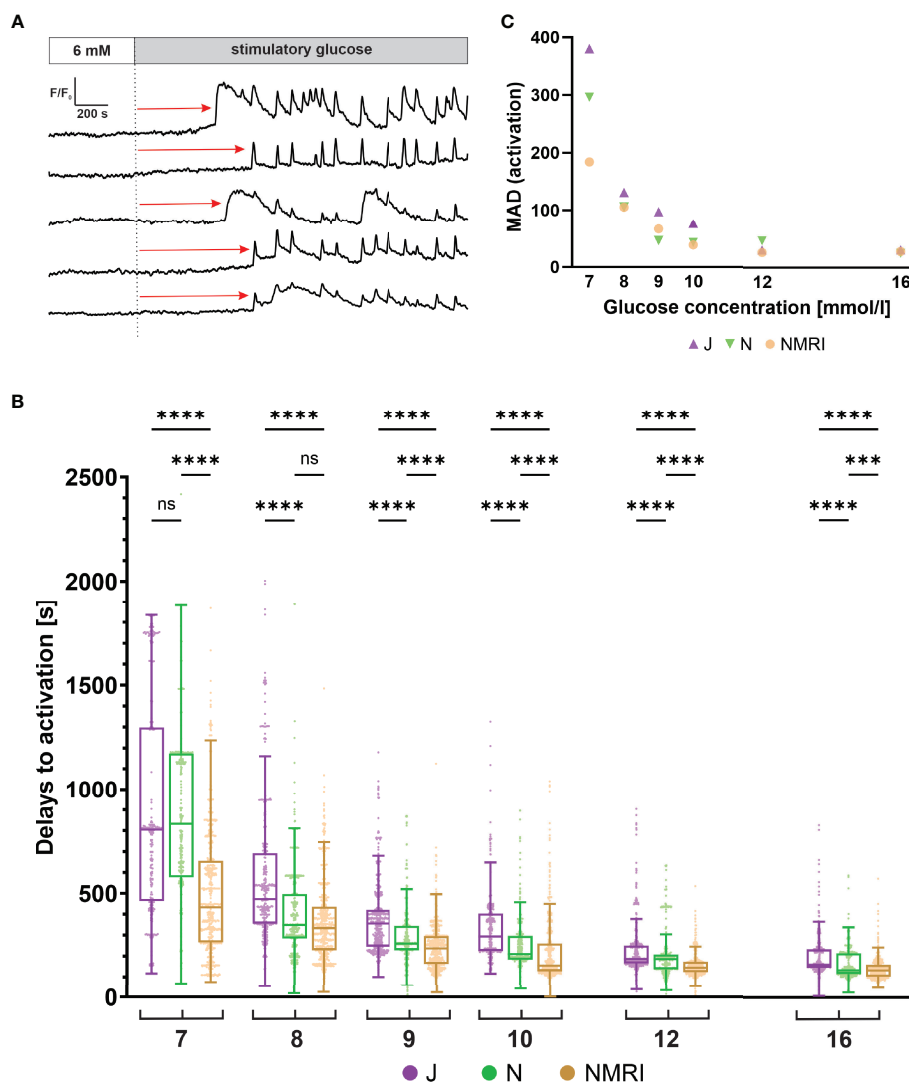
FIGURE 2 | Glucose-dependent activation delays of beta cells in C57BL/6J, C57BL/6N and NMRI mice. **(A)** Schematic representation of delays in activation (red arrow) measured as the time of perifusion of the islet with stimulatory glucose (dashed line) before the increase in $[Ca^{2+}]_i$ signal. **(B)** Delays to activation in C57BL/6J (median 805, 472, 357, 294, 186, and 156 s), C57BL/6N (median 833, 349, 260, 210, 185, 129 s), and NMRI (median 434, 334, 236, 155, 145, and 129 s) at 7-, 8-, 9-, 10-, 12-, and 16-mM glucose, respectively. **(C)** Variability of activation delays, expressed as median absolute deviation (MAD) after stimulation with 7-, 8-, 9-, 10-, 12-, and 16-mM glucose. MAD values (in seconds): C57BL/6J: 380 (7 mM), 131 (8 mM), 98 (9 mM), 76 (10 mM), 31 (12 mM), and 31 (16 mM), C57BL/6N: 296 (7 mM), 106 (8 mM), 46 (9 mM), 43 (10 mM), 47 (12 mM), and 25 (16 mM), NMRI: 184 (7 mM), 105 (8 mM), 66 (9 mM), 39 (10 mM), 26 (12 mM), and 28 (16 mM). Pooled data (coded as C57BL/6JC57BL/6NNMRI) from the following number of cells/islets/pancreas preparations: 239/9/6| 643/13/6| 743/13/6 (7mM glucose), 370/10/7| 876/8/5| 730/12/6 (8 mM glucose), 657/11/7| 851/9/6| 1091/12/6 (9 mM glucose), 521/9/6| 756/9/5| 1078/10/6 (10 mM glucose), 681/11/7| 759/11/6| 904/10/5 (12 mM glucose), and 725/11/5| 703/8/5| 1061/11/6 (16 mM glucose). Where present, the following symbols in indicate p-values: *p < 0.05, **p < 0.01, ***p < 0.001, ****p < 0.0001; ns, not significant.

by an average of 5.4%, 4.0%, and 6.3% per mM increase in glucose in C57BL/6J, C57BL/6N, and NMRI mice, respectively (**Figure 3D**). We did not observe a consistent difference in active time between the strains. The percentage of active time averaged 12.5% (C57BL/6J: 10.6%, C57BL/6N 16.0%, and NMRI: 10.9%) at 7 mM glucose and increased to an average of 44.7% (C57BL/6J: 44.4%, C57BL/6N 43.6%, and NMRI: 46.2%) at 16 mM glucose. To visualize the effect of glucose concentration on frequency and duration, we plotted the frequency of each oscillation against its respective duration, shown in **Figures 3E-G**. This approach separated the three strains with

respect to the coding of the glucose-stimulated $[Ca^{2+}]_i$ increase. The C57BL/6J strain depended on the change in frequency to increase the active time (**Figure 3E**). In contrast, stimulus strength predominantly modulated the duration of oscillations in C57BL/6N mice (**Figure 3F**). The NMRI strain shared properties of both (**Figure 3G**): The active time depended on an increase in frequency at ≤ 10 mM and the duration at > 10 mM glucose.

Finally, the interquartile range demonstrated a relatively large variability in all three parameters (**Figures 3B-D**). However, the variability seemed to change with glucose concentration when
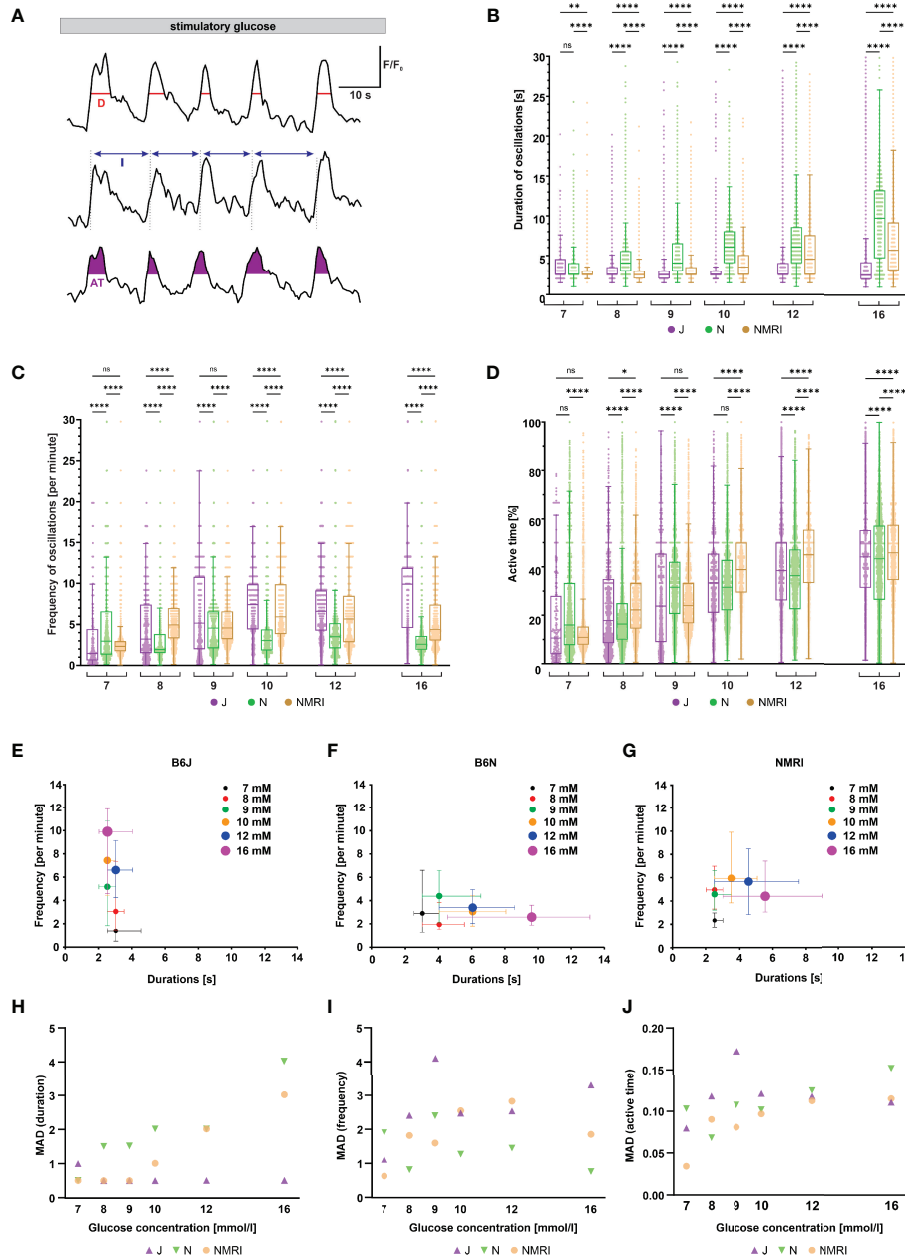
FIGURE 3 | Duration, frequency, and active time of fast oscillations during the plateau phase of beta cell response to glucose in C57BL/6J, C57BL/6N, and NMRI mice. **(A)** Schematic representation of analyzed parameters: oscillation duration **(D)**, frequency calculated from burst period (I), and active time (AT). Shown are three typical beta cells during the plateau phase of a response to 10 mM glucose. **(B)** Duration of oscillations in the three strains. C57BL/6J: median 3.0, 3.0, 2.5, 2.5, 3.0, and 2.5 s, C57BL/6N: 3.0, 4.0, 4.0, 6.1, 6.1, and 9.6 s, NMRI 2.5, 2.5, 2.5, 3.5, 4.5, and 5.5 s) in 7-, 8-, 9-, 10-, 12-, and 16-mM glucose, respectively. **(C)** Frequency of oscillations. C57BL/6J: median (1.5, 3.2, 5.2, 7.4, 6.6, and 9.6 min^{-1}, C57BL/6N: 3.0, 1.9, 4.6, 3.0, 3.5, and 2.6 min^{-1}, and NMRI: 2.3, 5.0, 4.6, 5.9, 5.7, and 4.4 min^{-1} in 7-, 8-, 9-, 10-, 12-, and 16-mM glucose, respectively. **(D)** Percentage of active time. C57BL/6J: median 10.6, 17.8, 23.8, 33.3, 38.5, and 44.4%, C57BL/6N: median 16.0, 16.4, 31.6, 31.6, 36.4, and 43.6%, and NMRI: 10.9, 22.2, 24.0, 38.9, 45.0, and 46.2% in 7-, 8-, 9-, 10-, 12-, and 16-mM glucose, respectively. **(E)** Oscillation durations as a function of respective frequency for B6J. **(F)** Oscillation durations as a function of respective frequency for B6N. **(G)** Oscillation durations as a function of respective frequency for NMRI. **(H)** MAD of oscillation durations. C57BL/6J: median 1.0, 0.5, 0.5, 0.5, 0.5, and 0.5 s, C57BL/6N: median 0.5, 1.5, 2.0, 2.0, and 4.0 s, NMRI: 0.5, 0.5, 0.5, 1.0, 2.0, and 3.0 s in 7-, 8-, 9-, 10-, 12-, and 16-mM glucose, respectively. **(I)** MAD of oscillation frequency. C57BL/6J: median 1.1, 2.4, 4.1, 2.5, 2.5, and 3.3 min^{-1}, C57BL/6N: median 1.9, 0.8, 2.4, 1.3, 1.4, and 0.8 min^{-1}, and NMRI: 0.6, 1.8, 1.6, 2.5, 2.8, and 1.9 min^{-1} in 7-, 8-, 9-, 10-, 12-, and 16-mM glucose, respectively. **(J)** MAD of percent active time. C57BL/6J: median 8.0, 11.8, 17.2, 12.1, 11.8, and 11.1%, C57BL/6N: 10.3, 6.8, 10.7, 10.2, 12.5, and 15.1%, and NMRI: median 3.4, 9.0, 8.1, 9.7, 11.2, and 11.5 in 7-, 8-, 9-, 10-, 12-, and 16-mM glucose, respectively. Pooled data (coded as C57BL/6JC57BL/6NNMRI) from the following number of cells/islets/pancreas preparations: 57/6/5| 325/11/6| 292/11/6 (7 mM glucose), 96/10/7| 671/8/5 381/10/5 (8 mM glucose), 246/8/7| 684/9/6| 574/10/6 (9 mM glucose), 250/8/5| 531/9/5| 677/9/6 (10 mM glucose), 322/10/7| 456/9/4| 310/7/5 (12 mM glucose), and 256/9/5| 414/7/5| 458/8/6 (16 mM glucose). Where present, the following symbols in indicate p-values: *p < 0.05, **p < 0.01, ***p < 0.001, ****p < 0.0001; ns, not significant.

the parameter was also concentration-dependent. More specifically, MAD of durations increased with glucose concentration for C57BL/6N (as did the absolute values) and ranged from a median MAD of 0.5 s at 7 mM to 4.0 s at 16 mM glucose, whereas MAD did not change for C57BL/6J (MAD ranged from 0.5 – 1.0 s with no clear trend). Conversely, MAD of frequencies increased in C57BL/6J (as did the absolute values) and ranged from 1.1 min^{-1} at 7 mM to 3.3 min^{-1} at 16 mM glucose, while the duration remained unaffected by glucose concentration (median MAD 0.8 – 2.4 min^{-1} with no clear trend). The NMRI strain exhibited both properties, increasing MAD of frequencies in the 7 – 10 mM glucose range (MAD 0.6 min^{-1} at 7 mM and 2.5 min^{-1} at 16 mM glucose), while MAD of durations increased above 10 mM glucose (MAD duration 3.0 s at 16 mM glucose). MAD of active time increased with increasing glucose concentrations in all strains spanning from 8.0, 10.3, and 3.5% in 7 mM glucose to 11.1, 15.1, and 11.5% in 16 mM for C57BL/6J, C57BL/6N, and NMRI mice. No systematic differences were observed in MAD of active time between inbred and outbred mice.

C57BL/6J Mice Deactivate Earlier Following Stimulation

Following glucose withdrawal, beta cells cease their oscillatory activity and return to the pre-stimulatory baseline $[Ca^{2+}]_i$ after a certain time delay (**Figure 4A**), as demonstrated previously for the NMRI strain (51, 54). To search for differences in the deactivation properties, we measured the deactivation delays of individual cells in all three strains. Generally, all three strains showed a concentration-dependent lengthening of deactivation delays (**Figure 4B**). However, in experiments using physiological glucose concentrations (7 - 10 mM glucose), an intermittent period of no activity in a portion of cells preceded or coincided with the withdrawal of the stimulus. The rest of the cells subsided their activity during and after stimulus withdrawal. The intermittent inactivity at the time of stimulus withdrawal resulted in a portion of negative deactivation delays. This effect was most noticeable in the C57BL/6J strain of mice, where the effect subsided glucose-dependently from 7 mM to 9 mM glucose and was negligible in higher (≥ 10 mM) glucose concentrations. Regardless of this phenomenon, increasing deactivation delays were observed, ranging from -208 s at 7 mM to 370 s at 16 mM glucose. The negative deactivation delays were also seen in C57BL/6N and NMRI mice, but much more rarely and mainly at concentrations of glucose < 8 mM. Similarly, for these two strains, the deactivation delays were glucose-dependent, ranging from a median of 133 s (C57BL/6N) and 178 s (NMRI) at 7 mM to 386 s (C57BL/6N) and 278 s (NMRI) at 16 mM glucose, respectively. Delays to deactivation were typically the longest in NMRI mice and the shortest in C57BL/6J mice. On average, the difference in median delays between NMRI and C57BL/6J mice was 47.1% (216.8% for 7 mM, 27.8% for 8 mM, 6.3% for 9 mM, 15.7% for 10 mM, 13.8% for 12 mM, and 2.3% for 16 mM). The C57BL/6N mice presented with an irregular deactivation pattern compared to C57BL/6J and NMRI mice, being the first to deactivate at some glucose concentrations (9 and 12 mM) and last in others (8 and 16 mM). However, their deactivation times

more closely resembled those of NMRI mice than C57BL/6J mice. More specifically, the average difference in median delays between NMRI and C57BL/6N mice was 9.9% (36.5% for 7 mM, -17.9% for 8 mM, 9.4% for 9 mM, 7.9% for 10 mM, 25.8% for 12 mM, and -2.0% for 16 mM).

Similarly to the activation, we observed relatively large variability in the deactivation delays (**Figure 4C**). We calculated the MAD of deactivation delays of cells in an islet and plotted pooled median values to display interstrain differences. Regarding the glucose concentration, the variability in the C57BL/6J expressed a U-shape with peaks observed at 7 mM (324 s) and 16 mM (170 s) glucose and with a nadir at 9 mM (49 s). The C57BL/6N and NMRI similarly exhibited a U-shaped dose-dependent response (C57BL/6N: peaks 74 s (7 mM) and 98 s (10 mM), NMRI: peaks 118 s (7 mM) and 153 s (12 mM)) that saturated (and even decreased) at higher stimulatory glucose concentrations. As with activations, no clear differences were observed between outbred and inbred strains.

DISCUSSION

Although animal models are generally accepted in (patho) physiological research of the pancreas, study outcomes were often generalized across taxonomic genera or even orders, assuming the same phenotypes and (patho)physiological mechanisms. This was an unsound assumption even for the most commonly used animal model *Mus musculus* (laboratory mouse), as several studies revealed significant differences between strains, especially in terms of animal size (58), glucose metabolism (22, 59), and even susceptibility to disease (60–63), to name a few. In the present study, we attempted to overcome this problem at least in part by systematically comparing the beta cell responses to glucose in the three most commonly used mouse models, the outbred NNT competent NMRI mice and the two inbred C57BL/6 substrains, i.e., the NNT deficient C57BL/6J and the NNT competent C57BL/6N mice. Apart from our own previous work (51), which was limited to the NMRI strain, to the best of our knowledge, the glucose-dependency of activation, activity, and deactivation of beta cells in intact islets of Langerhans has not been systematically studied.

To robustly assess how the analyzed beta cell characteristics relate to the *in vivo* glycemic status in these three strains, we also examined some basic physiological parameters. NMRI mice were larger and heavier than either of the C57BL/6 substrain, consistent with previous findings (64). Unsurprisingly, the same tendency was observed for the calculated BMI. The animal facility itself may be a contributing factor to metabolic rate and obesity in laboratory mice (65). However, all three strains of mice used in this experiment, were derived from the same animal facility. Non-fasting glucose did not differ between the strains, which was in accordance with some (23, 30), but not all previous results (66). The larger cross-sectional area of the islets in the NMRI strain may be due to a greater insulin requirement on account of larger animal size and contribute to normal glucose tolerance in these animals, given the very similar
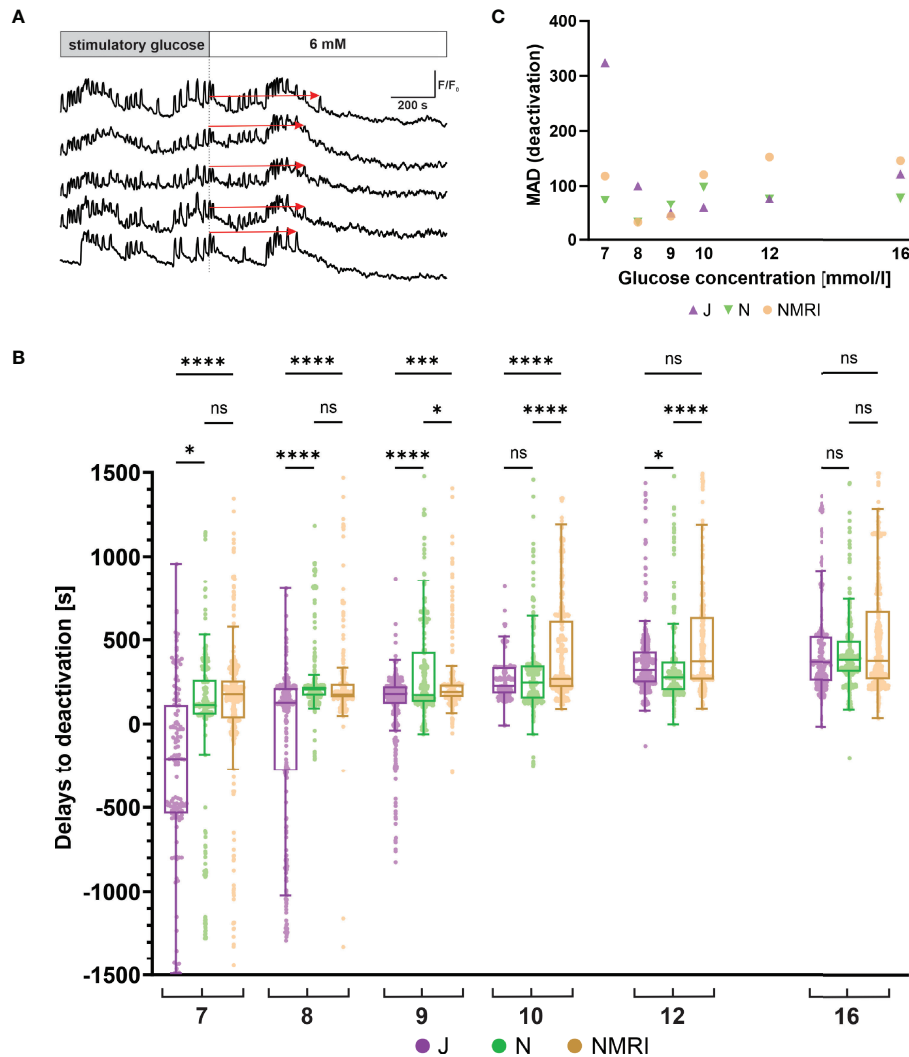
FIGURE 4 | Glucose-dependent deactivation delays of beta cells in C57BL/6J, C57BL/6N and NMRI strains. **(A)** Schematic representation of delays to deactivation (red arrow) measured as the time difference between end of stimulation (dashed line) and the last $[Ca^{2+}]_i$ oscillation. **(B)** Delays to deactivation in C57BL/6J (median -208, 126, 179, 227, 322, and 370 s), C57BL/6N (median 113, 206, 173, 248, 277, and 386 s), and NMRI (median 178, 175, 190, 269, 373, and 378 s) in 7-, 8-, 9-, 10-, 12-, and 16-mM glucose, respectively. **(C)** Variability in deactivation delays, expressed as median absolute deviation (MAD) after stimulation with 7-, 8-, 9-, 10-, 12-, and 16-mM glucose. MAD values (in seconds): C57BL/6J: 324 (7 mM), 100 (8 mM), 49 (9 mM), 59 (10 mM), 77 (12 mM), and 120 (16 mM), C57BL/6N: 74 (7 mM), 32 (8 mM), 65 (9 mM), 98 (10 mM), 76 (12 mM), and 77 (16 mM), NMRI: 118 (7 mM), 32 (8 mM), 43 (9 mM), 121 (10 mM), 153 (12 mM), and 145 (16 mM). Pooled data (coded as C57BL/6JC57BL/6NNMRI) from the following number of cells/islets/pancreas preparations: 133/6/5| 377/12/6| 472/12/6 (7mM glucose), 288/10/7| 832/8/5| 482/11/6 (8 mM glucose), 544/10/7| 700/9/5| 792/10/6 (9 mM glucose), 307/5/4| 711/9/5| 999/10/6 (10 mM glucose), 546/10/6| 676/11/6| 749/10/6 (12 mM glucose), and 657/11/6| 592/7/5| 809/10/6 (16 mM glucose). Where present, the following symbols in indicate p-values: *p < 0.05, **p < 0.01, ***p < 0.001, ****p < 0.0001; ns, not significant.

active time responses. Islet number clearly increases with body size across different species, but a possible contribution of islet size to increasing total islet mass in larger organisms is much less clear (4, 67–71). It has been reported that at least within species, islet size and architecture can change with increased demand due to growth and pregnancy (70, 72, 73). Islet areas of C57BL/6N and NMRI mice have not yet been systematically compared and our findings offer some support to the idea that increased islet size may account for at least a part of increased total islet mass in larger organisms. However, our cross-sectional data from a few slices are subject to many caveats. The most important is a

possible bias due to the selection of islets for calcium imaging. Future studies aimed at either random sampling of islet cross-sections within tissue slices, combined with insulin secretion data from the same slices, could provide more insight. However, it is worth mentioning that judging by previous work, the number of islets in NMRI and C57BL/6 mice of similar age probably does not differ significantly (72, 73).

Beta cells respond to a glucose stimulus with a time delay, a phenomenon attributed to the time needed for beta cells to metabolize glucose. Previously, large differences between individual cells following a random activation pattern have been

reported for the NMRI strain (51, 54). The present results confirm the previous findings in NMRI mice on an independent sample and further show that there is similar activation heterogeneity at the level of individual cells in all three substrains (**Figure 2B**). Importantly, beta cells show a progressive decrease in delays with increasing glucose concentration, a phenomenon termed advancement of beta cell activation, as previously demonstrated for the NMRI strain (51). The advancement of activation was observed in all three studied mouse strains (**Figure 2B**). The delay effect displayed a minimum at approximately 2 min, which agrees well with results observed in rats (74). However, the concentration dependence did not overlap when the three mouse strains were compared. Both inbred strains were right-shifted by 1.2 (C57BL/6J) and 0.9 mM (C57BL/6N) compared to NMRI mice (**Supplementary Figure 1**), suggesting that a higher glucose concentration is required for a comparable initiation of activation. Delays in activation were most pronounced in C57BL/6J mice resulting in several islets of C57BL/6J mice failing to respond to the established threshold for stimulatory glucose (7 mM). Although a comparable threshold concentration of 7.1 mM (**Figure 2B**) has been reported for insulin release from isolated islets offed and food-deprived C57BL/6J mice (75), a failure to report unresponsive islets, due to a biased search for responsive islets could have influenced concentration-dependence curves. The discrepancy in threshold concentration between our and previous results could also be attributed to differences in pre-stimulatory glucose concentration (76), a broadening of the curve of concentration dependence as a consequence of islet preparation, or other factors (77, 78).

There are a few possible reasons for differences in the observed shift towards a higher glucose concentration needed for the initiation of activation of both inbred strains. As reported previously, gap junctional coupling by connexin36 and the residual conductance after a complete closure of K_{ATP} channels with 5 mM intracellular ATP and extracellular application of 100 μM tolbutamide are greater in NMRI mice compared to C57Bl/6 mice (79). Moreover, the conductance of K_{ATP} channels in NMRI mice was shown to be lower, making beta cells less hyperpolarized. Consequently, membrane potential of beta cells in the NMRI mice may reach the threshold potential for the response to glucose and increased electrical activity faster, possibly making beta cells of the NMRI mice more responsive to lower glucose (79). Consistent with this hypothesis is the recent finding that in neonatal rat islets a decreased K_{ATP} channel could be responsible for the lower glucose threshold for insulin secretion (80). Another possible reason for differences in glucose concentration needed for activation/deactivation might lie in the size of the islet and the time that diffusion takes to reach the beta cells in the islet's center. However, when analyzing our data, we did not observe any correlation between the islet size and the activation/deactivation glucose concentration, contradicting the idea that diffusion is a decisive or limiting factor. Although one might suspect that prolonged diffusion time in bigger islets could result in a decreased responsiveness of big islets to glucose, this was not the case. In all glucose concentrations regardless of the mice strain, we observed small as well as big islets which responded either slower or faster to the glucose concentration change. These observations corroborate well with previous research (54).

After the initial activation described above, beta cells exhibit a plateau phase of $[Ca^{2+}]_i$ activity characterized by either fast, slow, or mixed oscillations (41, 81–83). How beta cells encode glucose concentration during this plateau phase is still a matter of debate. In tissue slices, fast oscillations are typically observed and previous studies that focused on the fast component provided conflicting results. Some showed an increase in the duration of individual oscillations having the same amplitude (84), while others reported increased frequency as glucose concentration increased (85). Many causes for this discrepancy are conceivable: sample preparation (damage due to enzymatic isolation of cells and islets, mechanical disruption due to microdissection of islets, lack of neuronal innervation in the tissue slice approach, poorly defined conditions for *in vivo* measurements), temporal resolution (high in electrophysiological recordings, low during confocal imaging), spatial resolution (single cell resolution when using patch pipette, islet resolution when using photomultiplier, multicellular resolution when using confocal imaging), the hormonal status of the animal (hormonal cycles in females), and inter-species and -strain differences, to name only a few. In this study, we compared plateau phases of beta cells in three strains of mice to account for the inter-strain effect. Surprisingly, the three strains of mice could be divided into three different categories, each with its own characteristic coding principles of either tuning the frequency, the duration, or a combination of both (**Figure 3**). Keeping in mind the limitation of non-ratiometric dyes as non-linear calcium reporters in mind, the coding seemed not to include the modulation of the amplitude of oscillations (**Supplementary Figure 2**). Beta cells from C57BL/6N mice exclusively modulated the duration, which tripled over the tested range (from ~ 3 s at 7 mM to ~ 10 s at 16 mM glucose), while the frequency remained unchanged (~ 3-4 min^{-1}). The C57BL/6J mice showed almost exactly the opposite characteristics: an exclusive modulation of oscillation frequency that increased approximately threefold over the tested range (from ~ 1.5 - 3 to ~ 9 min^{-1}). The NMRI strain exhibited the most complex coding strategy, switching from increases in frequency to increases in duration with increasing levels of stimulation. At 7 – 10 mM, the frequency increased approximately threefold (from ~ 2 in the lower to ~ 6 min^{-1} in the upper range), while durations remained unchanged. In yet higher glucose, durations increased about twofold (from ~ 2.5 s to ~ 5.5 s at 16 mM glucose), while frequency remained unchanged. To graphically represent the three coding modes, we plotted frequency as a function of respective durations over the tested range of concentrations (**Figures 3E-G**). This approach clearly separated the three substrains in terms of how the two parameters interacted: (i) exclusive frequency modulation in C57BL/6J mice, (ii) exclusive duration modulation in C57BL/6N mice, and (iii) a combination of both in NMRI mice. To our knowledge, this is the first report of such pronounced differences between substrains of the same species. The different properties should be carefully considered when interpreting the effects of various physiological or pharmacological secretagogues on oscillations to not miss a possible effect on frequency when there is no effect on duration, and when comparing the results from different studies to avoid the erroneous assumption that "a mouse is a mouse".

Similarity of the oscillatory behavior among islets (islet imprinting) from the same animal is crucial for the islet entrainment and the insulin pulsatility *in vivo* (86). The imprinting was related to the slow component of the oscillatory activity (typical period of several minutes), and seems not to include the fast component (83) studied here (**Supplemental Figure 3**). As suggested by recent theoretical and experimental studies, it is plausible that, due to a different mechanism, the imprinting of the slow component defines the frequency of the insulin oscillations, whereas the faster component sets the amplitude of the oscillations (83, 87). A study specifically designed at assessing the slow and fast component in different mouse strains is warranted to clarify this issue.

Surprisingly, the three strains shared remarkably similar curves of active time. Active time is best understood as the fraction of time that the calcium signal is elevated during repetitive oscillations. While active time is a product of oscillation frequency and duration, it is worth pointing out that an increase in oscillation duration alone does not necessarily increase active time as it may be accompanied by a reciprocal decrease in the frequency of oscillations. The values of ~ 15% at the threshold concentration increased to ~ 45% at 16 mM in an almost linear fashion in all substrains. In other words, for an increase in glucose concentration by 9 mM over the threshold level of 6 mM, the active time increased by 30%, or approximately 3% per 1 mM glucose. It is unclear how the increase in active time in all three mouse strains translates into effects on insulin secretion, per se, as only fast $[Ca^{2+}]_i$ oscillations were considered in this study. For the NMRI, we have recently shown that the active time of the fast oscillatory component almost perfectly followed the insulin secretion data (51). In contrast, the slow component was independent of glucose concentration (83). However, beta cells can most likely increase their active time to an even higher proportion if stimulated with even higher glucose concentrations than that used in this study. For instance, electrical activity of beta cells (88) was shown to approach saturation at 20 mM glucose or even higher and similar findings have been shown for insulin secretion (89–94). In fact, insulin secretion appears to increase well beyond what has been previously reported *via* $[Ca^{2+}]_i$-independent mechanisms (95). Considering active time increases similarly in all three mouse strains, but glucose-stimulated insulin release is impaired in C57BL/6J mice (19, 22), insulin secretion could be impaired not only upstream but also downstream of calcium at the level of the exocytotic machinery. This is not yet clear, as there are findings in favor of the former (19, 96) and the latter (66, 97). In future studies, it would be prudent to assess active time (and other oscillation parameters) also in 20 mM or higher glucose and also determine into more detail the relationship between active time estimated from electrical recordings and calcium oscillations at half-amplitude. The latter could theoretically yield lower values than the former and this discrepancy may account for slightly lower values of active time in this study compared with some previous findings (98, 99).

Finally, the deactivation properties of beta cells at the level of $[Ca^{2+}]_i$ have not yet been systematically examined for differences between strains. In all three strains, beta cell oscillatory $[Ca^{2+}]_i$

activity decreases when the stimulatory glucose is removed. However, it should be noted that in some islets, certain cells remained active to a lesser extent even 20 – 40 min after the end of stimulation, coinciding with an initial pause in $[Ca^{2+}]_i$ activity. This was observed mainly in the C57BL/6N and the NMRI mice, mostly at physiological glucose concentrations. However, quantification of these results could not be performed because it was impossible to establish strict criteria for categorizing these cells due to the varying length of the individual recordings. Therefore, this information was not included in our analysis. As for the cells that deactivated, data from all three strains of mice showed that the time required for deactivation increased with increasing glucose concentration. In some islets of the C57BL/6J strain, oscillations ceased even before the non-stimulatory glucose was reintroduced, resulting in negative delays in activation. This occurred at 7 – 9 mM stimulatory glucose concentrations, again indicating a shifted threshold for glucose-induced insulin secretion in the C57BL/6J strain. When stimulatory glucose was increased, delays in deactivation were prolonged and similar in all three groups.

The variability in activations, expressed by the median absolute deviation from the median, showed that variability was the highest at lower glucose concentrations, indicating that activations are much more dependent on activation thresholds within individual cells. As stimulatory glucose concentration increased, the variability of delays decreased, suggesting that activation of cells within an islet at supraphysiological concentrations is more strongly tied to the activity of other cells. In the plateau phase, variability increased with increasing glucose concentrations for the NMRI and C57BL/6N strains as far as durations are concerned but increased up to 12 mM glucose and decreased at 16 mM when looking at the variability of frequency. In C57BL/6J mice, variability stayed fairly constant in the case of durations, but the variability of oscillation frequencies increased steadily. Variability in active time increased with higher glucose concentrations for all strains. Variability in deactivations was higher at the threshold and in supraphysiological concentrations. We surprisingly did not observe any systematically higher variability in the outbred NMRI mice compared to the C57BL/6 substrains for any of the assessed parameters. This is somewhat at odds with recent blanket statement appeals for preferential use of inbred mouse strains over outbred stocks in research (8) and deserves further investigations in the future.

In an attempt to compare our findings in slices with previous findings in the same strains of mice in isolated islets, we wish to point out that to the best of our knowledge, the glucose-dependence and heterogeneity of the activation and deactivation phase have not been systematically analyzed in the past in isolated islets from different strains (51). With that being said, from some studies employing electrophysiological recordings or calcium imaging in islets from NMRI and C57BL/6J mice, the delays to activation upon stimulation and to deactivation upon cessation of stimulation seem to range from 1-5 minutes for glucose concentrations ranging from 8 mM to 20 mM (37, 40, 100–102), which is roughly within the range of values observed in our study. With respect to the plateau phase, there are more quantitative data available, and they suggest that in isolated islets the active time (also sometimes termed plateau

phase) increases over a very similar range of values for comparable increases in glucose (84, 103–105). Furthermore, in NMRI mice, the frequency of fast oscillations was reported to first increase and then drop with increasing glucose (105), whereas in C57Bl/6J mice (strain inferred due to KO animals used, not reported) it seems to monotonically increase with increasing glucose (85), which is consistent with our findings. However, more studies in isolated islets from different strains are needed to quantify possible differences between preparations and caution is warranted when extrapolating our findings to isolated islets.

There are further limitations to this study worth addressing. First, due to the rather large number of recordings needed to characterize the properties of responses across a range of glucose concentrations and strains, we constrained our experiments to 12–13-week-old male mice in three strains. In future studies, the dose-response relationships shall be investigated also at other ages, in female mice, as well as in other strains that have been or still are used in studying stimulus-secretion coupling in beta cells. This holds true for both control and disease conditions, e. g., genetic and dietary models of diabetes. Additionally, other cell types and other relevant physiological parameters could be addressed systematically, such as electrophysiological properties, coupling, exocytosis, and functional connectivity (51, 79, 106, 107). Second, while BMI is often considered as a surrogate measure of body fat, it is more accurately a measure of excess weight, rather than fat. For this reason, excision and weighing of fat-pad depots (25, 108) or use of Dual X-ray absorptiometry (DXA) (109, 110) would be more appropriate in future studies. A third concern might be the impact of the pre-stimulatory glucose concentration used, as the three strains have slightly different thresholds for stimulation (**Supplementary Figure 1**). This may imply that with the current protocol, the responses of cells are influenced by the relatively different degrees of stimulation. Therefore, a protocol where the pre-stimulatory and stimulatory glucose concentrations are set relative to the strain threshold rather than universally, might be beneficial in future studies (111, 112). Finally, we studied the responses to glucose only and it would be worth comparing across the strains the effects of other physiological and pharmacological secretagogues. This could be especially relevant since some, such as tolbutamide, seem to influence the activity of beta cells in a very similar manner as increasing glucose concentrations (104), whereas others, such as cAMP-elevating agents and acetylcholine, seem to increase the active time by increasing the frequency of oscillations in conditions when increasing glucose would lower it (104, 113–119).

CONCLUSIONS

In this study, we characterized for the first time glucose-stimulated $[Ca^{2+}]_i$ dynamics in two inbred mouse strains (C57BL/6J and C57BL/6N) most commonly used in islet research and confirmed our previous findings in outbred NMRI mice on a new independent sample (51, 54). We wish to point out that the use of inbred mice doesn't necessarily reduce variability, which is particularly true for experiments at physiological glucose concentrations. In future studies, findings on $[Ca^{2+}]_i$ dynamics

could be correlated with electrophysiological and insulin secretion data (something not yet possible in conjunction with the tissue slice). In addition, it will be interesting to see whether the $[Ca^{2+}]_i$ waves in the three substrains are comparable and what their functional connectivity patterns are (119), together with possible changes in dietary and genetic models of diabetes based on different backgrounds. Finally, our findings also underline the general importance of transparent experimental design, analysis, and interpretation of results (7). The apparent phenotypic differences between beta cells even within the same species should be accounted for when comparing the results of different studies and when examining the differences between mouse islets and islets of other species, since a mouse is not a mouse. Such an approach will hopefully help reconcile some of the currently conflicting views about beta cell physiology in mice, lead to a more accurate translation to humans, and ultimately help contribute to better mouse strain selection and reporting in beta cell physiology research.

DATA AVAILABILITY STATEMENT

The raw data supporting the conclusions of this article will be made available by the authors, without undue reservation.

ETHICS STATEMENT

The animal study was reviewed and approved by Administration for Food Safety, Veterinary Sector and Plant Protection (approval number: U34401-12/2015/3 and U34401-35/2018-2).

AUTHOR CONTRIBUTIONS

AS, JD, and VP designed the study. VP, LK, AS, MS, and JD performed the experiments. VP, JD, AS, MS, and LK analyzed the data. JD developed the software for analysis. VP, JD, AS, MS, and LK wrote the manuscript. All authors contributed to the article and approved the submitted version.

FUNDING

ACKNOWLEDGMENTS

SUPPLEMENTARY MATERIAL

The Supplementary Material for this article can be found online at: https://www.frontiersin.org/articles/10.3389/fendo.2022.867663/full#supplementary-material

REFERENCES

1. Rees DA, Alcolado JC. Animal Models of Diabetes Mellitus. *Diabet Med* (2005) 22:359–70. doi: 10.1111/j.1464-5491.2005.01499.x

2. Joost H-G, Al-Hasani H, Schürmann A. Animal Models in Diabetes Research. In: *Animal Models in Diabetes Research*. Totowa, NJ: Humana Press (2012). p. 161–74. doi: 10.1007/978-1-62703-068-7

3. Arrojo e Drigo R, Ali Y, Diez J, Srinivasan DK, Berggren P-O, Boehm BO. New Insights Into the Architecture of the Islet of Langerhans: A Focused Cross-Species Assessment. *Diabetologia* (2015) 58:2218–28. doi: 10.1007/s00125-015-3699-0

4. Dolenšek J, Rupnik MS, Stožer A. Structural Similarities and Differences Between the Human and the Mouse Pancreas. *Islets* (2015) 7:1–16. doi: 10.1080/19382014.2015.1024405

5. Skelin Klemen M, Dolenšek J, Slak Rupnik M, Stožer A. The Triggering Pathway to Insulin Secretion: Functional Similarities and Differences Between the Human and the Mouse β Cells and Their Translational Relevance. *Islets* (2017) 9:109–39. doi: 10.1080/19382014.2017.1342022

6. Cefalu WT. Animal Models of Type 2 Diabetes: Clinical Presentation and Pathophysiological Relevance to the Human Condition. *ILAR J* (2006) 47:186–98. doi: 10.1093/ilar.47.3.186

7. Alquier T, Poitout V. Considerations and Guidelines for Mouse Metabolic Phenotyping in Diabetes Research. *Diabetologia* (2018) 61:526. doi: 10.1007/S00125-017-4495-9

8. Festing MFW. Evidence Should Trump Intuition by Preferring Inbred Strains to Outbred Stocks in Preclinical Research. *ILAR J* (2014) 55:399–404. doi: 10.1093/ilar/ilu036

9. Chia R, Achilli F, Festing MFW, Fisher EMC. The Origins and Uses of Mouse Outbred Stocks. *Nat Genet* (2005) 37:1181–6. doi: 10.1038/ng1665

10. Festing MWF. Phenotypic Variability of Inbred and Outbred Mice. *Nature* (1976) 263:230–2. doi: 10.1038/263230a0

11. Festing MFW. Inbred Strains Should Replace Outbred Stocks in Toxicology, Safety Testing, and Drug Development. *Toxicol Pathol* (2010) 38:681–90. doi: 10.1177/0192623310373776

12. Biggers JD, Claringbold PJ. Why Use Inbred Lines? *Nature* (1954) 174:596–7. doi: 10.1038/174596a0

13. Jensen VS, Porsgaard T, Lykkesfeldt J, Hvid H. Rodent Model Choice has Major Impact on Variability of Standard Preclinical Readouts Associated With Diabetes and Obesity Research. *Am J Transl Res* (2016) 8:3574–84.

14. Tuttle AH, Philip VM, Chesler EJ, Mogil JS. Comparing Phenotypic Variation Between Inbred and Outbred Mice. *Nat Methods* (2018) 15:994–6. doi: 10.1038/s41592-018-0224-7

15. Mekada K, Abe K, Murakami A, Nakamura S, Nakata H, Moriwaki K, et al. Genetic Differences Among C57BL/6 Substrains. *Exp Anim* (2009) 58:141–9. doi: 10.1538/expanim.58.141

16. Simon MM, Greenaway S, White JK, Fuchs H, Gailus-Durner V, Wells S, et al. A Comparative Phenotypic and Genomic Analysis of C57BL/6J and C57BL/6N Mouse Strains. *Genome Biol* (2013) 14:R82. doi: 10.1186/gb-2013-14-7-r82

17. Matsuo N, Takao K, Nakanishi K, Yamasaki N, Tanda K, Miyakawa T. Behavioral Profiles of Three C57BL/6 Substrains. *Front Behav Neurosci* (2010) 4:29. doi: 10.3389/fnbeh.2010.00029

18. Aston-Mourney K, Wong N, Kebede M, Zraika S, Balmer L, McMahon JM, et al. Increased Nicotinamide Nucleotide Transhydrogenase Levels Predispose to Insulin Hypersecretion in a Mouse Strain Susceptible to Diabetes. *Diabetologia* (2007) 50:2476–85. doi: 10.1007/s00125-007-0814-x

19. Toye AA, Lippiat JD, Proks P, Shimomura K, Bentley L, Hugill A, et al. A Genetic and Physiological Study of Impaired Glucose Homeostasis Control in C57BL/6J Mice. *Diabetologia* (2005) 48:675–86. doi: 10.1007/s00125-005-1680-z

20. Freeman HC, Hugill A, Dear NT, Ashcroft FM, Cox RD. Deletion of Nicotinamide Nucleotide Transhydrogenase A New Quantitive Trait Locus Accounting for Glucose Intolerance in C57BL/6J Mice. *Diabetes* (2006) 55:2153–6. doi: 10.2337/db06-0358

21. Huang TT, Naeemuddin M, Elchuri S, Yamaguchi M, Kozy HM, Carlson EJ, et al. Genetic Modifiers of the Phenotype of Mice Deficient in Mitochondrial Superoxide Dismutase. *Hum Mol Genet* (2006) 15:1187–94. doi: 10.1093/hmg/ddl034

22. Kaku K, Fiedorek FT, Province M, Permutt MA. Genetic Analysis of Glucose Tolerance in Inbred Mouse Strains. Evidence for Polygenic Control. *Diabetes* (1988) 37:707–13. doi: 10.2337/diab.37.6.707

23. Fergusson G, Éthier M, Guévremont M, Chrétien C, Attané C, Joly E, et al. Defective Insulin Secretory Response to Intravenous Glucose in C57Bl/6J Compared to C57Bl/6N Mice. *Mol Metab* (2014) 3:848–54. doi: 10.1016/j.molmet.2014.09.006

24. Hull RL, Willard JR, Struck MD, Barrow BM, Brar GS, Andrikopoulos S, et al. High Fat Feeding Unmasks Variable Insulin Responses in Male C57BL/6 Mouse Substrains. *J Endocrinol* (2017) 233:53–64. doi: 10.1530/JOE-16-0377

25. Wong N, Blair AR, Morahan G, Andrikopoulos S. The Deletion Variant of Nicotinamide Nucleotide Transhydrogenase (Nnt) Does Not Affect Insulin Secretion or Glucose Tolerance. *Endocrinology* (2010) 151:96–102. doi: 10.1210/en.2009-0887

26. Alonso LC, Watanabe Y, Stefanovski D, Lee EJ, Singamsetty S, Romano LC, et al. Simultaneous Measurement of Insulin Sensitivity, Insulin Secretion, and the Disposition Index in Conscious Unhandled Mice. *Obesity* (2012) 20:1403–12. doi: 10.1038/oby.2012.36

27. Nicholson A, Reifsnyder PC, Malcolm RD, Lucas C, MacGregor GR, Zhang W, et al. Diet-Induced Obesity in Two C57BL/6 Substrains With Intact or Mutant Nicotinamide Nucleotide Transhydrogenase (Nnt) Gene. *Obesity* (2010) 18:1902–5. doi: 10.1038/oby.2009.477

28. Rendina-Ruedy E, Hembree KD, Sasaki A, Davis MR, Lightfoot SA, Clarke SL, et al. A Comparative Study of the Metabolic and Skeletal Response of C57BL/6J and C57BL/6N Mice in a Diet-Induced Model of Type 2 Diabetes. *J Nutr Metab* (2015) 2015:1–13. doi: 10.1155/2015/758080

29. Fisher-Wellman KH, Ryan TE, Smith CD, Gilliam LAA, Lin C-T, Reese LR, et al. A Direct Comparison of Metabolic Responses to High-Fat Diet in C57BL/6J and C57BL/6NJ Mice. *Diabetes* (2016) 65:3249–61. doi: 10.2337/db16-0291

30. Ahren B, Scheurink A. Marked Hyperleptinemia After High-Fat Diet Associated With Severe Glucose Intolerance in Mice. *Eur J Endocrinol* (1998) 139:461–7. doi: 10.1530/eje.0.1390461

31. Pacini G, Thomaseth K, Ahrén B. Dissociated Effects of Glucose-Dependent Insulinotropic Polypeptide vs Glucagon-Like Peptide–1 on β-Cell Secretion and Insulin Clearance in Mice. *Metabolism* (2010) 59:988–92. doi: 10.1016/j.metabol.2009.10.021

32. Fontaine DA, Davis DB. Attention to Background Strain Is Essential for Metabolic Research: C57BL/6 and the International Knockout Mouse Consortium. *Diabetes* (2016) 65:25–33. doi: 10.2337/db15-0982

33. Grodsky GM, Bennett LL. Cation Requirements for Insulin Secretion in the Isolated Perfused Pancreas. *Diabetes* (1966) 15:910–0. doi: 10.2337/diab.15.12.910

34. Wollheim CB, Sharp GW. Regulation of Insulin Release by Calcium. *Physiol Rev* (1981) 61:914–73. doi: 10.1152/physrev.1981.61.4.914

35. Gilon P, Chae H-Y, Rutter GA, Ravier MA. Calcium Signaling in Pancreatic β-Cells in Health and in Type 2 Diabetes. *Cell Calcium* (2014) 56:340–61. doi: 10.1016/j.ceca.2014.09.001

36. Hamilton A, Vergari E, Miranda C, Tarasov AI. Imaging Calcium Dynamics in Subpopulations of Mouse Pancreatic Islet Cells. *J Vis Exp* (2019) 2019:e59491. doi: 10.3791/59491

37. Gilon P, Henquin JC. Influence of Membrane Potential Changes on Cytoplasmic Ca2+ Concentration in an Electrically Excitable Cell, the Insulin-Secreting Pancreatic B-Cell. *J Biol Chem* (1992) 267:20713–20. doi: 10.1016/s0021-9258(19)36744-4

38. Santos RM, Rosario LM, Nadal A, Garcia-Sancho J, Soria B, Valdeolmillos M. Widespread Synchronous [Ca2+]i Oscillations Due to Bursting Electrical Activity in Single Pancreatic Islets. *Pflügers Arch - Eur J Physiol* (1991) 418:417–22. doi: 10.1007/bf00550880

39. Dolenšek J, Špelič D, Klemen M, Žalik B, Gosak M, Rupnik M, et al. Membrane Potential and Calcium Dynamics in Beta Cells From Mouse Pancreas Tissue Slices: Theory, Experimentation, and Analysis. *Sensors* (2015) 15:27393–419. doi: 10.3390/s151127393

40. Gilon P, Shepherd RM, Henquin JC. Oscillations of Secretion Driven by Oscillations of Cytoplasmic Ca2+ as Evidences in Single Pancreatic Islets. *J Biol Chem* (1993) 268:22265–8. doi: 10.1016/S0021-9258(18)41522-0

41. Bergsten P, Grapengiesser E, Gylfe E, Tengholm A, Hellman B. Synchronous Oscillations of Cytoplasmic Ca2+ and Insulin Release in Glucose-Stimulated

Pancreatic Islets. *J Biol Chem* (1994) 269:8749–53. doi: 10.1016/S0021-9258 (17)37032-1

42. Jonkers FC, Jonas J-C, Gilon P, Henquin J-C. Influence of Cell Number on the Characteristics and Synchrony of Ca^{2+} Oscillations in Clusters of Mouse Pancreatic Islet Cells. *J Physiol* (1999) 520:839–49. doi: 10.1111/j.1469-7793.1999.00839.x

43. Nilsson T, Hallberg A, Hellman B, Berggren O. Characterization of the Inositol 1,4,5-Trisphosphate-Induced Ca^{2+} Release in Pancreatic β-Cells. *Biochem J* 248(1987):329–36. doi: 10.1042/bj2480329

44. Grapengiesser E, Gylfe E, Hellman B. Dual Effect of Glucose on Cytoplasmic Ca2+ in Single Pancreatic β-Cells. *Biochem Biophys Res Commun* (1988) 150:419–25. doi: 10.1016/0006-291X(88)90537-2

45. Li L, Trifunovic A, Kohler M, Wang Y, Petrovic Berglund J, Illies C, et al. Defects in -Cell Ca2+ Dynamics in Age-Induced Diabetes. *Diabetes* (2014) 63:4100–14. doi: 10.2337/db13-1855

46. Tanaka T, Nagashima K, Inagaki N, Kioka H, Takashima S, Fukuoka H, et al. Glucose-Stimulated Single Pancreatic Islets Sustain Increased Cytosolic ATP Levels During Initial Ca2+ Influx and Subsequent Ca2+ Oscillations. *J Biol Chem* (2014) 289:2205–16. doi: 10.1074/jbc.M113.499111

47. Zhang M, Goforth P, Bertram R, Sherman A, Satin L. The Ca2+ Dynamics of Isolated Mouse β-Cells and Islets: Implications for Mathematical Models. *Biophys J* (2003) 84:2852–70. doi: 10.1016/S0006-3495(03)70014-9

48. Chen C, Chmelova H, Cohrs CM, Chouinard JA, Jahn SR, Stertmann J, et al. Alterations in β-Cell Calcium Dynamics and Efficacy Outweigh Islet Mass Adaptation in Compensation of Insulin Resistance and Prediabetes Onset. *Diabetes* (2016) 65:2676–85. doi: 10.2337/db15-1718

49. Johnston NR, Mitchell RK, Haythorne E, Pessoa MP, Semplici F, Ferrer J, et al. Beta Cell Hubs Dictate Pancreatic Islet Responses to Glucose. *Cell Metab* (2016) 24:389–401. doi: 10.1016/j.cmet.2016.06.020

50. Westacott MJ, Ludin NWF, Benninger RKP. Spatially Organized β-Cell Subpopulations Control Electrical Dynamics Across Islets of Langerhans. *Biophys J* (2017) 113:1093–108. doi: 10.1016/j.bpj.2017.07.021

51. Stožer A, Skelin Klemen M, Gosak M, Križančić Bombek L, Pohorec V, Slak Rupnik M, et al. Glucose-Dependent Activation, Activity, and Deactivation of Beta Cell Networks in Acute Mouse Pancreas Tissue Slices. *Am J Physiol Metab* (2021) 321:E305–23. doi: 10.1152/ajpendo.00043.2021

52. Gargiulo S, Gramanzini M, Megna R, Greco A, Albanese S, Manfredi C, et al. Evaluation of Growth Patterns and Body Composition in C57Bl/6J Mice Using Dual Energy X-Ray Absorptiometry. *BioMed Res Int* (2014) 2014:1–11. doi: 10.1155/2014/253067

53. Speier S, Rupnik M. A Novel Approach to in Situ Characterization of Pancreatic β-Cells. *Pflügers Arch* (2003) 446:553–8. doi: 10.1007/s00424-003-1097-9

54. Stožer A, Dolenšek J, Rupnik MS. Glucose-Stimulated Calcium Dynamics in Islets of Langerhans in Acute Mouse Pancreas Tissue Slices. *PloS One* (2013) 8:e54638. doi: 10.1371/journal.pone.0054638

55. Stožer A, Dolenšek J, Križančić Bombek L, Pohorec V, Slak Rupnik M, Klemen MS. Confocal Laser Scanning Microscopy of Calcium Dynamics in Acute Mouse Pancreatic Tissue Slices. *JoVE* (2021):e62293. doi: 10.3791/62293

56. Sebaugh JL. Guidelines for Accurate EC50/IC50 Estimation. *Pharm Stat* (2011) 10:128–34. doi: 10.1002/pst.426

57. Stožer A, Dolenšek J, Skelin Klemen M, Slak Rupnik M. Cell Physiology in Tissue Slices - Studying Beta Cells in the Islets of Langerhans. *Acta Medico-Biotechnica* (2013) 6:20–32.

58. Reed DR, Bachmanov AA, Tordoff MG. Forty Mouse Strain Survey of Body Composition. *Physiol Behav* (2007) 91:593–600. doi: 10.1016/j.physbeh.2007.03.026

59. Andrikopoulos S, Blair AR, Deluca N, Fam BC, Proietto J. Evaluating the Glucose Tolerance Test in Mice. *Am J Physiol Metab* (2008) 295:E1323–32. doi: 10.1152/ajpendo.90617.2008

60. Coleman DL, Hummel KP. The Influence of Genetic Background on the Expression of the Obese (Ob) Gene in the Mouse. *Diabetologia* (1973) 9:287–93. doi: 10.1007/BF01221856

61. Paigen B, Morrow A, Brandon C, Mitchell D, Holmes P. Variation in Susceptibility to Atherosclerosis Among Inbred Strains of Mice. *Atherosclerosis* (1985) 57:65–73. doi: 10.1016/0021-9150(85)90138-8

62. Leiter EH. The Genetics of Diabetes Susceptibility in Mice. *FASEB J* (1989) 3:2231–41. doi: 10.1096/fasebj.3.11.2673897

63. Hartner A. Strain Differences in the Development of Hypertension and Glomerular Lesions Induced by Deoxycorticosterone Acetate Salt in Mice. *Nephrol Dial Transplant* (2003) 18:1999–2004. doi: 10.1093/ndt/gfg299

64. Matysková R, Maletínská L, Maixnerová J, Pirník Z, Kiss A, Zelezná B. Comparison of the Obesity Phenotypes Related to Monosodium Glutamate Effect on Arcuate Nucleus and/or the High Fat Diet Feeding in C57BL/6 and NMRI Mice. *Physiol Res* (2008) 57:727–34. doi: 10.33549/physiolres.931274

65. Corrigan JK, Ramachandran D, He Y, Palmer CJ, Jurczak MJ, Chen R, et al. A Big-Data Approach to Understanding Metabolic Rate and Response to Obesity in Laboratory Mice. *Elife* (2020) 9:1–34. doi: 10.7554/eLife.53560

66. Santos LRB, Muller C, de Souza AH, Takahashi HK, Spégel P, Sweet IR, et al. NNT Reverse Mode of Operation Mediates Glucose Control of Mitochondrial NADPH and Glutathione Redox State in Mouse Pancreatic β-Cells. *Mol Metab* (2017) 6:535–47. doi: 10.1016/j.molmet.2017.04.004

67. Hellman B. Actual Distribution of the Number and Volume of the Islets of Langerhans in Different Size Classes in Non-Diabetic Humans of Varying Ages. *Nature* (1959) 184:1498–9. doi: 10.1038/1841498a0

68. Hellman B, Brolin S, Hellerström C, Hellman K. The Distribution Pattern of the Pancreatic Islet Volume in Normal and Hyperglycaemic Mice. *Acta Endocrinol (Copenh)* (1961) 36:609–16. doi: 10.1530/acta.0.0360609

69. Bouwens L, Rooman I. Regulation of Pancreatic Beta-Cell Mass. *Physiol Rev* (2005) 85:1255–70. doi: 10.1152/physrev.00025.2004

70. Kim A, Miller K, Jo J, Kilimnik G, Wojcik P, Hara M. Islet Architecture: A Comparative Study. *Islets* (2009) 1:129–36. doi: 10.4161/isl.1.2.9480

71. Steiner DJ, Kim A, Miller K, Hara M. Pancreatic Islet Plasticity: Interspecies Comparison of Islet Architecture and Composition. *Islets* (2010) 2:135–45. doi: 10.4161/isl.2.3.11815

72. Bonnevie-Nielsen V, Skovgaard LT, Lernmark A. Beta-Cell Function Relative to Islet Volume and Hormone Content in the Isolated Perfused Mouse Pancreas. *Endocrinology* (1983) 112:1049–56. doi: 10.1210/endo-112-3-1049

73. Parsons JA, Bartke A, Sorenson RL. Number and Size of Islets of Langerhans in Pregnant, Human Growth Hormone-Expressing Transgenic, and Pituitary Dwarf Mice: Effect of Lactogenic Hormones. *Endocrinology* (1995) 136:2013–21. doi: 10.1210/endo.136.5.7720649

74. Pralong WF, Bartley C, Wollheim CB. Single Islet Beta-Cell Stimulation by Nutrients: Relationship Between Pyridine Nucleotides, Cytosolic Ca2+ and Secretion. *EMBO J* (1990) 9:53–60. doi: 10.1002/j.1460-2075.1990.tb08079.x

75. Chen N-G, Tassava TM, Romsos DR. Threshold for Glucose-Stimulated Insulin Secretion in Pancreatic Islets of Genetically Obese (Ob/Ob) Mice is Abnormally Low. *J Nutr* (1993) 123:1567–74. doi: 10.1093/jn/123.9.1567

76. Rebelato E, Santos LR, Carpinelli AR, Rorsman P, Abdulkader F. Short-Term High Glucose Culture Potentiates Pancreatic Beta Cell Function. *Sci Rep* (2018) 81(8):1–9. doi: 10.1038/s41598-018-31325-5

77. Henquin JC, Jonas JC, Gilon P. Culture Duration and Conditions Affect the Oscillations of Cytoplasmic Calcium Concentration Induced by Glucose in Mouse Pancreatic Islets. *Diabetologia* (1994) 37:1007–14. doi: 10.1007/s001250050211

78. Jonkers FC, Henquin JC. Measurements of Cytoplasmic Ca2+ in Islet Cell Clusters Show That Glucose Rapidly Recruits β-Cells and Gradually Increases the Individual Cell Response. *Diabetes* (2001) 50:540–50. doi: 10.2337/diabetes.50.3.540

79. Speier S, Gjinovci A, Charollais A, Meda P, Rupnik M. Cx36-Mediated Coupling Reduces Beta-Cell Heterogeneity, Confines the Stimulating Glucose Concentration Range, and Affects Insulin Release Kinetics. *Diabetes* (2007) 56:1078–86. doi: 10.2337/db06-0232

80. Yang J, Hammoud B, Li C, Ridler A, Yau D, Kim J, et al. Decreased KATP Channel Activity Contributes to the Low Glucose Threshold for Insulin Secretion of Rat Neonatal Islets. *Endocrinology* (2021) 162. doi: 10.1210/endocr/bqab121

81. Valdeolmillos M, Santos RM, Contreras D, Soria B, Rosario LM. Glucose-Induced Oscillations of Intracellular Ca2+ Concentration Resembling Bursting Electrical Activity in Single Mouse Islets of Langerhans. *FEBS Lett* (1989) 259:19–23. doi: 10.1016/0014-5793(89)81484-X

82. Bertram R, Satin L, Zhang M, Smolen P, Sherman A. Calcium and Glycolysis Mediate Multiple Bursting Modes in Pancreatic Islets. *Biophys J* (2004) 87:3074. doi: 10.1529/BIOPHYSJ.104.049262

83. Zmazek J, Klemen MS, Markovič R, Dolenšek J, Marhl M, Stožer A, et al. Assessing Different Temporal Scales of Calcium Dynamics in Networks of

Beta Cell Populations. *Front Physiol* (2021) 12:612233. doi: 10.3389/fphys.2021.612233

84. Antunes CM, Salgado AP, Rosário LM, Santos RM. Differential Patterns of Glucose-Induced Electrical Activity and Intracellular Calcium Responses in Single Mouse and Rat Pancreatic Islets. *Diabetes* (2000) 49:2028–38. doi: 10.2337/diabetes.49.12.2028

85. Lebreton F, Pirog A, Belouah I, Bosco D, Berney T, Meda P, et al. Slow Potentials Encode Intercellular Coupling and Insulin Demand in Pancreatic Beta Cells. *Diabetologia* (2015) 58:1291–9. doi: 10.1007/s00125-015-3558-z

86. Nunemaker CS, Dishinger JF, Dula SB, Wu R, Merrins MJ, Reid KR, et al. Glucose Metabolism, Islet Architecture, and Genetic Homogeneity in Imprinting of [Ca2+]i and Insulin Rhythms in Mouse Islets. *PloS One* (2009) 4:e8428. doi: 10.1371/journal.pone.0008428

87. Bertram R, Satin LS, Sherman AS. Closing in on the Mechanisms of Pulsatile Insulin Secretion. *Diabetes* (2018) 67:351–9. doi: 10.2337/dbi17-0004

88. Drews G, Krippeit-Drews P, Düfer M. Electrophysiology of Islet Cells. In: *The Islets of Langerhans*. Dordrech: Springer (2010). p. 115–63. doi: 10.1007/978-90-481-3271-3_7

89. Ashcroft SJ, Bassett JM, Randle PJ. Insulin Secretion Mechanisms and Glucose Metabolism in Isolated Islets. *Diabetes* (1972) 21:538–45. doi: 10.2337/diab.21.2.S538

90. Gao ZY, Drews G, Nenquin M, Plant TD, Henquin JC. Mechanisms of the Stimulation of Insulin Release by Arginine-Vasopressin in Normal Mouse Islets. *J Biol Chem* (1990) 265:15724–30. doi: 10.1016/S0021-9258(18)55457-0

91. Henquin J-C, Nenquin M, Stiernet P, Ahren B. In Vivo and *In Vitro* Glucose-Induced Biphasic Insulin Secretion in the Mouse. *Diabetes* (2006) 55:441–51. doi: 10.2337/diabetes.55.02.06.db05-1051

92. Benninger RKP, Head WS, Zhang M, Satin LS, Piston DW. Gap Junctions and Other Mechanisms of Cell-Cell Communication Regulate Basal Insulin Secretion in the Pancreatic Islet. *J Physiol* (2011) 589:5453–66. doi: 10.1113/jphysiol.2011.218909

93. Low JT, Mitchell JM, Do OH, Bax J, Rawlings A, Zavortink M, et al. Glucose Principally Regulates Insulin Secretion in Mouse Islets by Controlling the Numbers of Granule Fusion Events Per Cell. *Diabetologia* (2013) 56:2629–37. doi: 10.1007/s00125-013-3019-5

94. Alcazar O, Buchwald P. Concentration-Dependency and Time Profile of Insulin Secretion: Dynamic Perifusion Studies With Human and Murine Islets. *Front Endocrinol (Lausanne)* (2019) 10:680. doi: 10.3389/fendo.2019.00680

95. Gerber KM, Whitticar NB, Rochester DR, Corbin KL, Koch WJ, Nunemaker CS. The Capacity to Secrete Insulin Is Dose-Dependent to Extremely High Glucose Concentrations: A Key Role for Adenylyl Cyclase. *Metabolites* (2021) 11:401. doi: 10.3390/metabo11060401

96. Freeman H, Shimomura K, Cox RDD, Ashcroft FMM. Nicotinamide Nucleotide Transhydrogenase: A Link Between Insulin Secretion, Glucose Metabolism and Oxidative Stress. *Biochem Soc Trans* (2006) 34:806–10. doi: 10.1042/BST0340806

97. Close A, Chae H, Jonas J-C. The Lack of Functional Nicotinamide Nucleotide Transhydrogenase Only Moderately Contributes to the Impairment of Glucose Tolerance and Glucose-Stimulated Insulin Secretion in C57BL/6J vs C57BL/6N Mice. *Diabetologia* (2021) 64:2550–61. doi: 10.1007/s00125-021-05548-7

98. Meissner H, Atwater I. The Kinetics of Electrical Activity of Beta Cells in Response to a "Square Wave" Stimulation With Glucose or Glibenclamide. *Horm Metab Res* (1976) 8:11–6. doi: 10.1055/s-0028-1093685

99. Henquin JC. Regulation of Insulin Release by Ionic and Electrical Events in B Cells. *Horm Res* (1987) 27:168–78. doi: 10.1159/000180806

100. Gonzalez A, Merino B, Marroquí L, Ñeco P, Alonso-Magdalena P, Caballero-Garrido E, et al. Insulin Hypersecretion in Islets From Diet-Induced Hyperinsulinemic Obese Female Mice is Associated With Several Functional Adaptations in Individual β-Cells. *Endocrinology* (2013) 154:3515–24. doi: 10.1210/EN.2013-1424

101. Irles E, Ñeco P, Lluesma M, Villar-Pazos S, Santos-Silva JC, Vettorazzi JF, et al. Enhanced Glucose-Induced Intracellular Signaling Promotes Insulin Hypersecretion: Pancreatic Beta-Cell Functional Adaptations in a Model of Genetic Obesity and Prediabetes. *Mol Cell Endocrinol* (2015) 404:46–55. doi: 10.1016/j.mce.2015.01.033

102. Kravets V, Dwulet JM, Schleicher WE, Hodson DJ, Davis AM, Pyle L, et al. Functional Architecture of the Pancreatic Islets Reveals First Responder Cells Which Drive the First-Phase [Ca2+] Response. *bioRxiv* (2021):2020.12.22.424082. doi: 10.1101/2020.12.22.424082

103. Meissner HP, Schmelz H. Membrane Potential of Beta-Cells in Pancreatic Islets. *Pflügers Arch - Eur J Physiol* (1974) 351:195–206. doi: 10.1007/BF00586918

104. Cook DL, Ikeuchi M. Tolbutamide as Mimic of Glucose on β-Cell Electrical Activity: ATP-Sensitive K+ Channels as Common Pathway for Both Stimuli. *Diabetes* (1989) 38:416–21. doi: 10.2337/diab.38.4.416

105. Henquin JC. Adenosine Triphosphate-Sensitive K+ Channels may Not be the Sole Regulators of Glucose-Induced Electrical Activity in Pancreatic B-Cells. *Endocrinology* (1992) 131:127–31. doi: 10.1210/endo.131.1.1611991

106. Huang Y-C, Rupnik M, Gaisano HY. Unperturbed Islet α-Cell Function Examined in Mouse Pancreas Tissue Slices. *J Physiol* (2011) 589:395–408. doi: 10.1113/jphysiol.2010.200345

107. Klemen MS, Dolenšek J, Stožer A, Rupnik MS. Measuring Exocytosis in Endocrine Tissue Slices. In: *Exocytosis Methods*. Totowa, NJ: Humana Press (2014). p. 127–46. doi: 10.1007/978-1-62703-676-4_7

108. Wu Y, Lee MJ, Ido Y, Fried SK. High-Fat Diet-Induced Obesity Regulates MMP3 to Modulate Depot- and Sex-Dependent Adipose Expansion in C57BL/6J Mice. *Am J Physiol - Endocrinol Metab* (2017) 312:E58–71. doi: 10.1152/ajpendo.00128.2016

109. Nagy TR, Clair A-L. Precision and Accuracy of Dual-Energy X-Ray Absorptiometry for Determining in Vivo Body Composition of Mice. *Obes Res* (2000) 8:392–8. doi: 10.1038/oby.2000.47

110. Sjögren K, Hellberg N, Bohlooly-Y M, Savendahl L, Johansson MS, Berglindh T, et al. Body Fat Content Can Be Predicted In Vivo in Mice Using a Modified Dual-Energy X-Ray Absorptiometry Technique. *J Nutr* (2001) 131:2963–6. doi: 10.1038/oby.2000.47

111. Licko V. Threshold Secretory Mechanism: A Model of Derivative Element in Biological Control. *Bull Math Biol* (1973) 35:51–8. doi: 10.1016/S0092-8240(73)80007-2

112. Pedersen MG, Toffolo GM, Cobelli C. Cellular Modeling: Insight Into Oral Minimal Models of Insulin Secretion. *Am J Physiol Metab* (2010) 298:E597–601. doi: 10.1152/ajpendo.00670.2009

113. Cook DL, Crill WE, Porte D. Glucose and Acetylcholine Have Different Effects on the Plateau Pacemaker of Pancreatic Islet Cells. *Diabetes* (1981) 30:558–61. doi: 10.2337/diab.30.7.558

114. Ikeuchi M, Cook DL. Glucagon and Forskolin Have Dual Effects Upon Islet Cell Electrical Activity. *Life Sci* (1984) 35:685–91. doi: 10.1016/0024-3205(84)90264-9

115. Henquin JC, Garcia M-C, Bozem M, Hermans MP, Nenquin M. Muscarinic Control of Pancreatic B Cell Function Involves Sodium-Dependent Depolarization and Calcium Influx*. *Endocrinology* (1988) 122:2134–42. doi: 10.1210/endo-122-5-2134

116. Gilon P, Henquin JC. Mechanisms and Physiological Significance of the Cholinergic Control of Pancreatic Beta-Cell Function. *Endocr Rev* (2001) 22:565–604. doi: 10.1210/edrv.22.5.0440

117. Klemen MS, Dolenšek J, Bombek LK, Pohorec V, Gosak M, Rupnik MS, et al. The Effect of cAMP and the Role of Epac2A During Activation, Activity, and Deactivation of Beta Cell Networks. (2021). doi: 10.20944/PREPRINTS202105.0064.V1

118. Sluga N, Postić S, Sarikas S, Huang YC, Stožer A, Slak Rupnik M. Dual Mode of Action of Acetylcholine on Cytosolic Calcium Oscillations in Pancreatic Beta and Acinar Cells in Situ. *Cells* (2021) 10:1580. doi: 10.3390/cells10071580

119. Šterk M, Križančić Bombek L, Skelin Klemen M, Slak Rupnik M, Marhl M, Stožer A, et al. NMDA Receptor Inhibition Increases, Synchronizes, and Stabilizes the Collective Pancreatic Beta Cell Activity: Insights Through Multilayer Network Analysis. *PloS Comput Biol* (2021) 17:e1009002. doi: 10.1371/journal.pcbi.1009002

Publisher's Note: All claims expressed in this article are solely those of the authors and do not necessarily represent those of their affiliated organizations, or those of the publisher, the editors and the reviewers. Any product that may be evaluated in

this article, or claim that may be made by its manufacturer, is not guaranteed or endorsed by the publisher.